ADVANCED MATERIALS
www.advmat.de

A Continuous Gradient Colloidal Glass

*Marius Schöttle, Tobias Lauster, Lukas J. Roemling, Nicolas Vogel, and Markus Retsch**

Colloidal crystals and glasses manipulate light propagation depending on their chemical composition, particle morphology, and mesoscopic structure. This light–matter interaction has been intensely investigated, but a knowledge gap remains for mesostructures comprising a continuous property gradient of the constituting particles. Here, a general synthetic approach to bottom-up fabrication of continuous size gradient colloidal ensembles is introduced. First, the technique synthesizes a dispersion with a specifically designed gradual particle size distribution. Second, self-assembly of this dispersion yields a photonic colloidal glass with a continuous size gradient from top to bottom. Local and bulk characterization methods are used to highlight the significant potential of this mesostructure, resulting in vivid structural colors along, and in superior light scattering across the gradient. The process describes a general pathway to mesoscopic gradients. It can expectedly be transferred to a variety of other particle-based systems where continuous gradients will provide novel physical insights and functionalities.

1. Introduction

Structured materials show perceptible photonic properties when the characteristic length scale is similar to the wavelength of visible light. The interaction of photons with a periodically changing refractive index (n) in photonic crystals (PCs) creates a dispersion relation with wave-vector dependent gaps analogous to that of electrons in semiconductors.[1] These stop bands are the cause of characteristic, iridescent structural colors.[2] From sensors to optical metamaterials, increasingly complex structures allow tailoring of these properties.[3,4] However, many are only accessible via simulations or in the microwave range,[5,6] others are limited to high-n materials.[7]

Complementary to the phenomenon of ballistic light transport in ordered structures is the dispersive light diffusion in photonic glasses (PGs).[8–10] These jammed packings of monodisperse, dielectric spheres show coherent scattering due to Mie resonances and short-range order.[11,12] Because of the isotropic nature, the resulting colors are angle-independent.[13,14] Particle size and morphology, such as core-shell and hollow sphere structures, have been shown to influence the optical properties and provide tunable scattering and broadband reflectance of PGs.[15–19] Recently, anisotropic particles have also been shown to be useful for the adjustment of the scattering properties of the ensembles.[20,21]

Hierarchical structural design can introduce further complexity to particulate system.[22] For example, multilayer PC films with a cross-plane, stepwise change of the lattice constant show properties not found in single-component systems. These range from broadband reflectivity[23] to angular selectivity.[24] However, fabrication methods are often tedious and typically apply physical vapor deposition or repetitive colloidal assembly.[25,26] Without precise optimization, the latter can suffer from degradation of preformed layers and delamination. Further issues include incoherent light scattering at the interfaces and small sample sizes.

Despite the intense research on photonic crystals and glasses, one major category of colloidal mesostructure has received surprisingly little attention: continuous gradient structures. Continuous gradients in colloidal assemblies is an emerging topic, with few examples and approaches being reported in literature. Gradual changes, e.g., in the interparticle distance or composition can be formed via centrifugation,[27,28] post-assembly deformation[29] or modified coating procedures.[30,31] From a fundamental point of view, a better physical understanding of photonic materials with gradually changing properties needs to be developed and compared to experimental results.[32–34] To our knowledge, no experimental realization of a photonic colloidal assembly with a continuous particle size gradient has been presented to date. To achieve such a structure, two major challenges need to be addressed: First, particle dispersions with precise control of size and a continuous size variation need to be reliably available. Second, self-assembly must retain, not mix, the particle size gradient and immobilize the particles gradually in the colloidal ensemble.

Here, we provide a solution to both challenges that conceivably can also be applied to other (functional) particles. This general approach to continuous gradient colloidal glasses will add a missing piece to the field of colloidal mesostructures and opens a new field for photonic engineering and beyond. At the heart

M. Schöttle, T. Lauster, M. Retsch
Department of Chemistry
University of Bayreuth
Universitätsstr. 30, 95447 Bayreuth, Germany
E-mail: markus.retsch@uni-bayreuth.de
L. J. Roemling, N. Vogel
Insitute of Particle Technology
Friedrich-Alexander University Erlangen-Nürnberg
91058 Erlangen, Germany
The ORCID identification number(s) for the author(s) of this article can be found under https://doi.org/10.1002/adma.202208745.

DOI: 10.1002/adma.202208745

of our work is a controlled emulsion extraction process (CrEEP) that enables us to store the time-dependent size increase of monodisperse latex particles in a thin extraction tube, where laminar flow prevails. Subsequent filtration assembly translates the gradient dispersion into a film with a fully continuous, cross-plane gradient of the particle size. First, we present the synthesis method and then show the characteristics of the 3D self-assembled colloidal gradient material.

2. Results and Discussion

Surfactant-free emulsion polymerization is an established method for the preparation of monodisperse latex particle suspensions.[35,36] Further control can be obtained via a semibatch process by first preparing seed particles that then increase in size when more monomer is added.[37,38] In our CrEEP-approach (Figures S1 and S2, Supporting Information), the monomer is added gradually, and the growing particle suspension is simultaneously extracted into a thin tube. The resulting time-dependent change of the particle diameter is thereby stored in the extraction tube and turned into a positional dependency. Slow extraction and the small diameter of the tube provide controlled laminar flow. To verify the controlled nature of this process, we show that the reaction rate of the emulsion polymerization is fast compared the rate of monomer addition by evaluating the kinetics of the particle growth during seed synthesis (Figure S3, Supporting information). Mixing is further inhibited by fractionation via the injection of air bubbles as separators inside the tube. Thereby the monodisperse nature inherent to the emulsion polymerization is maintained. Analogous experiments without injection of air result in a slightly less ordered assembly (Figure S4, Supporting information). The air bubbles have the additional benefit of quenching the remaining initiator molecules with ambient oxygen, inhibiting any further polymerization. The fact that the continuous particle growth and extraction take place in the same reactor as the seed synthesis ensures reproducible starting conditions. Combined with the slow monomer addition, this results in a highly controlled reaction. Ultimately, a large number of equidistant fractions (in this case 110) are retained in the tube (**Figure 1**a). We examine every 10th fraction via dynamic light scattering (DLS) and correlate it to the respective reaction time during the extraction process (Figure 1b,c). We observe a near-linear increase of the hydrodynamic particle diameter and a low polydispersity throughout the synthesis. Both confirm the high degree of control that is necessary for the self-assembly process, which is dramatically influenced by both size and size distribution. In our example, we prepare a diameter range between 220–310 nm to specifically target photonic materials in the visible range. In combination with the number of fractions, this implies a sub-nm step size between neighboring fractions. Naturally, this is smaller than the size distribution of any given latex particle synthesis. Consequently, this constitutes a smooth and gradual size increase, a feature not accessible using a multi-pot approach.

To demonstrate the quality of fractions obtained via CrEEP, we induce self-assembly via heated drop-casting. The formation of PCs with structural colors dependent on the diameter of the particles becomes apparent via white light microscopy (Figure 1d). Brilliant colors ranging from blue to red can be observed. Due to the fcc symmetry and the concomitant *k*-vector dependency of the optical stop-band, these are inherently angle-dependent. Increasing the angle between light source and observer causes a blue shift of all 12 drop-cast spots (Figure 1e) and verifies the crystallinity. Further optical characterization with normal incidence reflectance μ-UV–vis spectroscopy (Figure 1f) elucidates the size-dependent properties. As the particle diameter increases, the stop-band peak gradually shifts to higher wavelengths. The position of the peak with respect to the reaction time of the corresponding fraction follows a linear trend (Figure 1g). Considering the linear dependency of the lattice spacing and wavelength in the Bragg–Snell Equation,[25] this corroborates the similar trend observed for the DLS results. Scanning electron microscopy (SEM) images of four selected PCs (Figure 1h) illustrate the monodisperse nature and hexagonal symmetry as well as the controlled increase of the particle size. An overview SEM image (Figure S5, Supporting Information) shows large domain sizes. Altogether this preliminary evaluation of the extracted fractions shows that the gradual increase of the particle size can be retained in a thin tube via CrEEP. Prevention of mixing thereby ensures that the monodisperse nature is maintained and allows self-assembly to form photonic structures.

After the CrEEP, a gradient colloidal dispersion is stored inside the extraction tube in a size-sorted manner. We now present a straightforward self-assembly process to transform this gradient dispersion into a colloidal glass with a smooth and continuous gradient. Our semicontinuous filtration technique involves dilution and subsequent filtration of each fraction. This allows us to fabricate a free-standing colloidal glass film with a gradually increasing particle size from top to bottom (**Figure 2**a; Figure S6a, Supporting Information). A sample 3.5 cm in diameter and with a thickness of 110 ± 5 μm is thereby obtained (Figure S6b, Supporting Information).

We demonstrate the successful fabrication of the intended gradient colloidal glass by laser scanning confocal microscopy (LSCM)[39] across the edge of a broken gradient film. An overlay of the height image obtained via laser-scanning and white light microscopy images from various focal positions provides a simple and intuitive impression (Figure 2b; Figure S7, Supporting Information). Complementary to the colorful appearance observed for self-assembled particles of separate fractions, we find structural colors continuously ranging from blue to red, reminiscent of a rainbow. The top and bottom faces appear blue and red, respectively, corresponding to the particle size of the first and last fraction. The addition of a broadband absorber is known to counteract the effect of diffuse scattering.[40] We, therefore, improve the saturation of the side-view structural colors by a thin layer of carbon (10 nm) on the surface of the cross section (Figure S8, Supporting information). While the colloidal glass filtration is conducted in a semicontinuous way, we do not observe any layering or stepwise particle size increase. As outlined in the gradient dispersion synthesis, the mean particle size changes with <1 nm from fraction to fraction, which is too small to be resolved analytically. Another advantage of the filtration approach is that a large sample can be prepared with homogeneous gradient properties. The colloidal

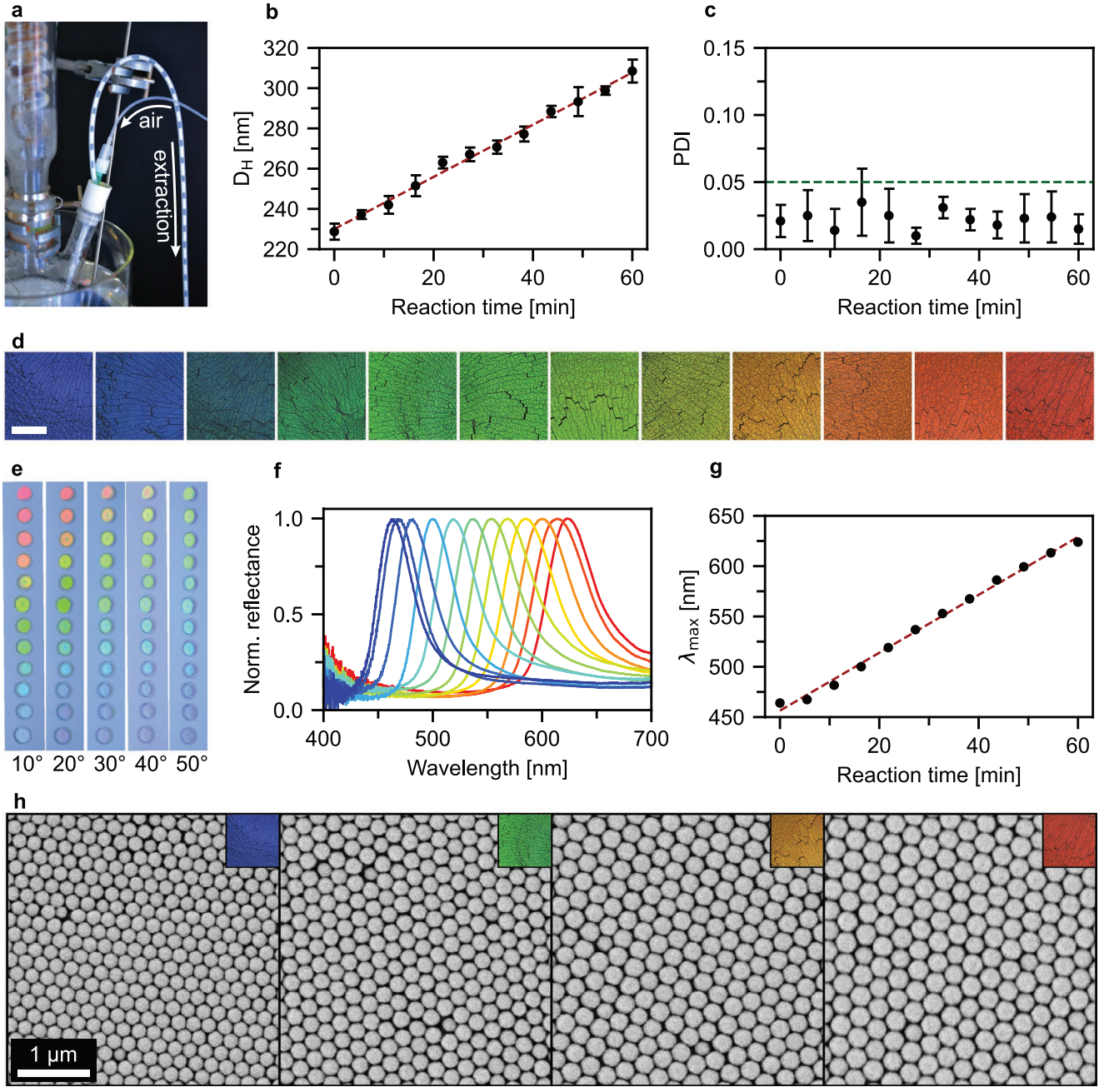

Figure 1. Characterization of equidistant fractions after the controlled emulsion extraction process (CrEEP). a) Snapshot of fractions during the extraction process showing even separation by air bubbles. b,c) Hydrodynamic diameter (D_H) and polydispersity index (PDI) obtained from DLS measurements of every 10th fraction. The reaction time noted here corresponds to the CrEEP starting with the gradual monomer addition. A linear fit shown in red elucidates the highly controlled nature of the gradual seeded growth. The polydispersity remains below 5% and is independent of the reaction time. d) Light microscopy images of these fractions after drop-casting showing size-dependent structural colors typical for colloidal crystals. Scale bar: 100 µm e) Photographs of the samples measured in (d) at different angles between camera and light source. f) µ-UV–vis reflectance spectra of the drop-cast fractions showing a gradual red-shift of the stop-band as the particle size increases. g) Peak position of the stop-band versus reaction time showing a linear relation. This stands in accordance with the DLS measurements and particle size. h) SEM images of selected drop-cast fractions. Insets show the corresponding light microscopy images. Both the increase in absolute size, as well as the consistently monodisperse nature, can be observed in the self-assembled colloidal crystals showing hexagonal symmetry.

gradient and hence the photonic properties are identical when examining cross sections via LSCM at several different macroscopic positions along the length of the filtered film (Figure S9, Supporting Information).

SEM images of selected positions along the cross section (Figure 2c) provide structural insights into the origin of colors in the gradient. The filtration assembly forces random aggregation of particles and thus a disordered structure. We

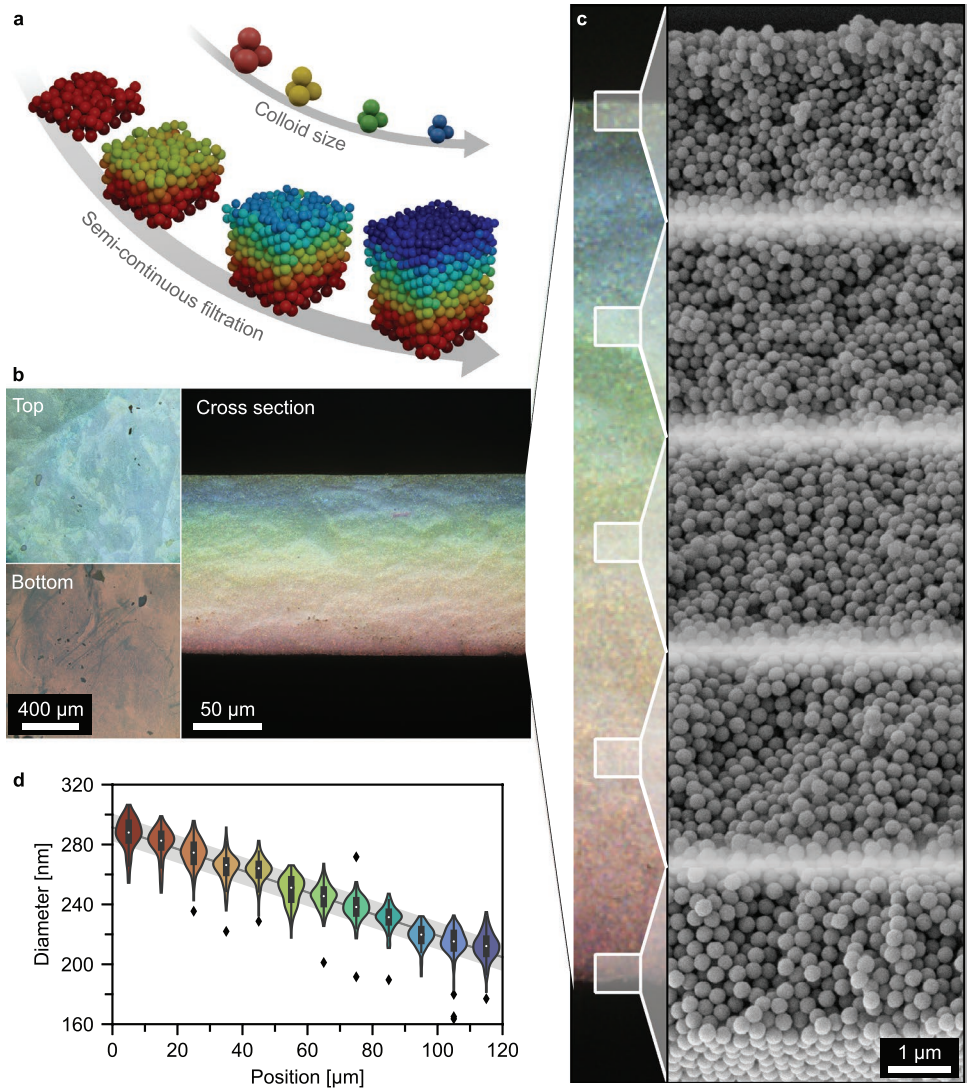

Figure 2. Gradient photonic glass prepared via semicontinuous filtration. a) Schematic illustration of the *z*-gradient structure resulting from the gradual assembly process. b) Light microscopy images of the top and bottom surface as well as the cross section showing the gradual transition of structural color throughout the entire visible spectrum. c) Representative SEM images of the colloidal assembly at the positions indicated in the cross-section. d) Size distribution of particles at equidistant positions along the gradient as obtained from the SEM images in Figure S10 (Supporting Information). At each position, more than 100 particles were measured. Outliers are shown as black diamonds.

attribute this to the fast kinetics of the filtration process and the absence of capillary forces.[22] The result is a photonic glass that consists of monodisperse, dielectric Mie scatterers and shows a position-dependent resonance frequency. Measurement of particle diameters at equidistant *z*-positions along the cross section allowed statistical evaluation of the change in size (Figure 2d; Figure S10, Supporting Information). Two important observations can be made here: 1) The position-dependent particle size shows a linear trend. This, once more, emphasizes the high degree of control during synthesis and assembly. We achieve this linearity by careful optimization of the CrEEP (details are outlined in Figure S11, Supporting Information). 2) At any given *z*-position, all particles are nearly monodisperse, underlining the performance of the fractionation in our process. The efficiency of fractionation is better than the polydispersity of the emulsion polymerization itself; hence the overlap of individual fractions is continuous. The result is one of the significant features presented in this work: the circumvention of discrete steps in a gradient particle assembly. The photonic glass shown here is consequently a fully continuous gradient structure.

For a full characterization analogous to that of discrete fractions, we show local µ-UV–vis reflectance spectra at equidistant positions along the gradient material (**Figure 3**a; Figure S12, Supporting Information). As the particle size increases, the reflectance peak shows a gradual red shift (Figure 3b). This positional dependency is linear, (Figure 3c) which correlates with the linear change in diameter examined via SEM evaluation. Compared to the spectra of colloidal crystals in Figure 1f, the width of these peaks is significantly larger. We attribute this to the short-range order and also partly to the fact that the measurement averages over a range

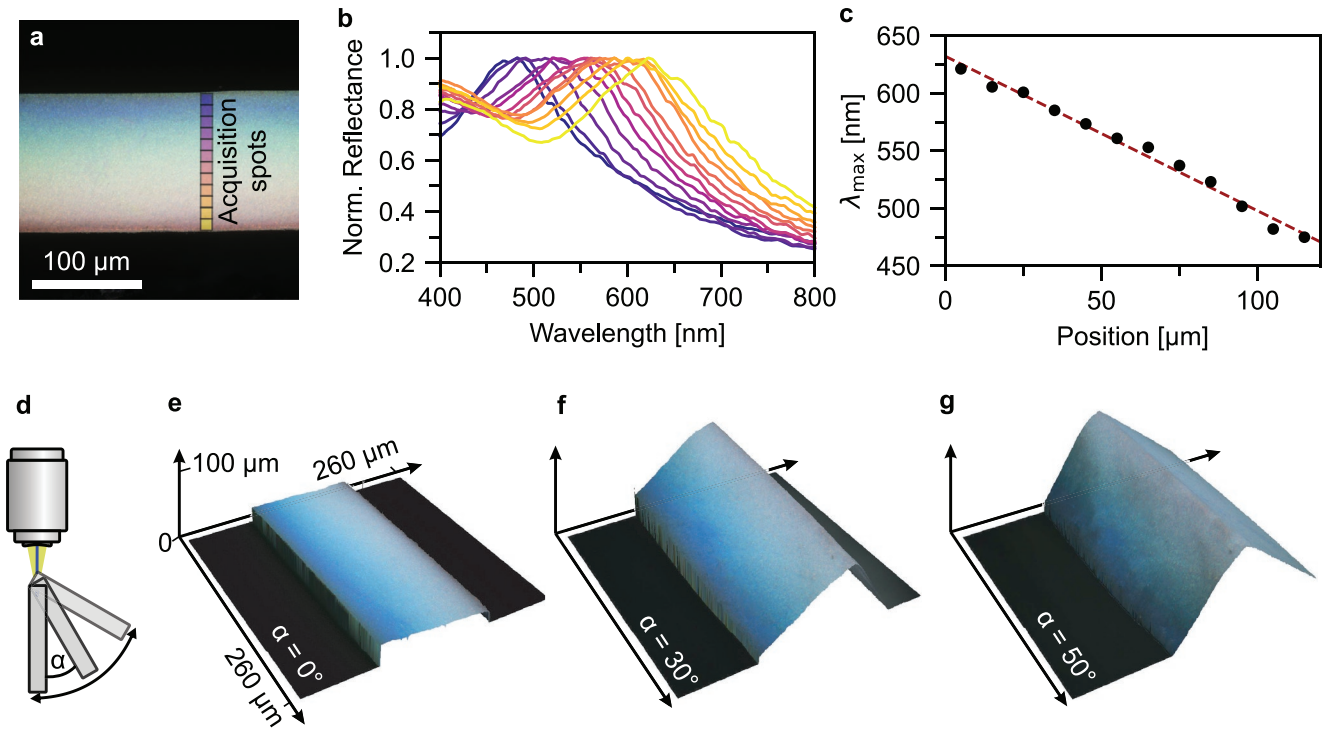

Figure 3. Local optical characterization of the gradient photonic glass. a) Microscopy image of a carbon-coated cross-section illustrating the spot size and position where individual spectra were obtained. b) Local spectra and c) wavelengths of the peak maxima showing a linear red-shift from the top to the bottom of the gradient. d) Microscopy setup used to examine different viewing angles of one gradient cross-section to prove the angle independence of the structural colors. e,f) Resulting overlay of height and white light microscopy images obtained via LSCM of a sample tilted between 0 and 50°. The color range of the gradient remains between blue and red, independent of the viewing angle.

of 10 µm, thereby covering a particle size increase of ≈8 nm in each area. The latter effect becomes more obvious when increasing the spot size (Figure S13d, Supporting Information). Averaging over half the cross section thereby naturally results in further peak broadening. Spectra obtained from samples without carbon-coating show stronger diffuse scattering, most visible toward smaller wavelengths (Figure S13a,c, Supporting Information).

The fact that isotropic colloidal assemblies exhibit no discrete peaks in Fourier space and, therefore, produce non-iridescent colors can be a significant advantage.[16] We examine this property by tilting the cross section of a gradient photonic glass under a microscope and conducting LSCM measurements at different viewing angles from 0 to 50° (Figure 3d–g; Figure S14, Supporting Information). This approach is similar to previously shown characterization methods of colloidal suprapartícles.[41] Unlike the results obtained for the iridescent colloidal crystals in Figure 1e, the coloration remains unchanged and ranges between blue and red at all viewing angles. In summary, the local characterization reveals that the gradient colloidal glass exhibits angle-independent reflectivity throughout the visible spectrum.

We now compare the diffuse reflectance from the top surface of the colloidal gradient glass with different reference samples (**Figure 4**a–f) to establish how the continuous mesostructure affects the optical properties. Homogeneous, non-gradient samples are prepared via filtration of pure small (224 nm) and large (304 nm) particles, respectively. Additionally, these particles are used for the fabrication of a statistical, binary mixture as well as a bilayer sample. The CrEEP technique is applied to prepare two different samples: 1) a statistical "gradient mixture" via mixing of all fractions and subsequent filtration and 2) the continuous gradient material discussed in Figure 2 and Figure 3. The two CrEEP-syntheses are shown to be identical via UV–vis spectroscopy and DLS measurements of the particles in the respective first and last fractions (Figure S15, Supporting Information). The film thickness is 112 ± 3 µm throughout all samples (Figure S16, Supporting Information).

The single-component sample consisting of small particles shows an intense blue color, whereas the large particles result in a less saturated red appearance. The latter is more compromised by diffuse light scattering and, therefore, appears fainter. The UV–vis diffuse reflectance spectra of these samples show distinct peaks at 420 and 580 nm, respectively (Figure 4g), as expected from the increase in diameter.[42]

Next, the two disordered structures, both binary and gradient mixture, are compared. Microscopy images of cross sections of the two show a white color. However, the reflectance spectra reveal a pronounced difference (Figure 4h), even though both samples comprise particles in the same size range. The binary mixture almost exclusively results in a profile characteristic for diffuse scattering. A slight shoulder at 550 nm hints toward a rather weak contribution of coherent scattering. Conversely, in the case of the gradient mixture, a distinct peak at 515 nm can be observed. This lies roughly in the middle of the peaks observed for the pure small and large particles, respectively.

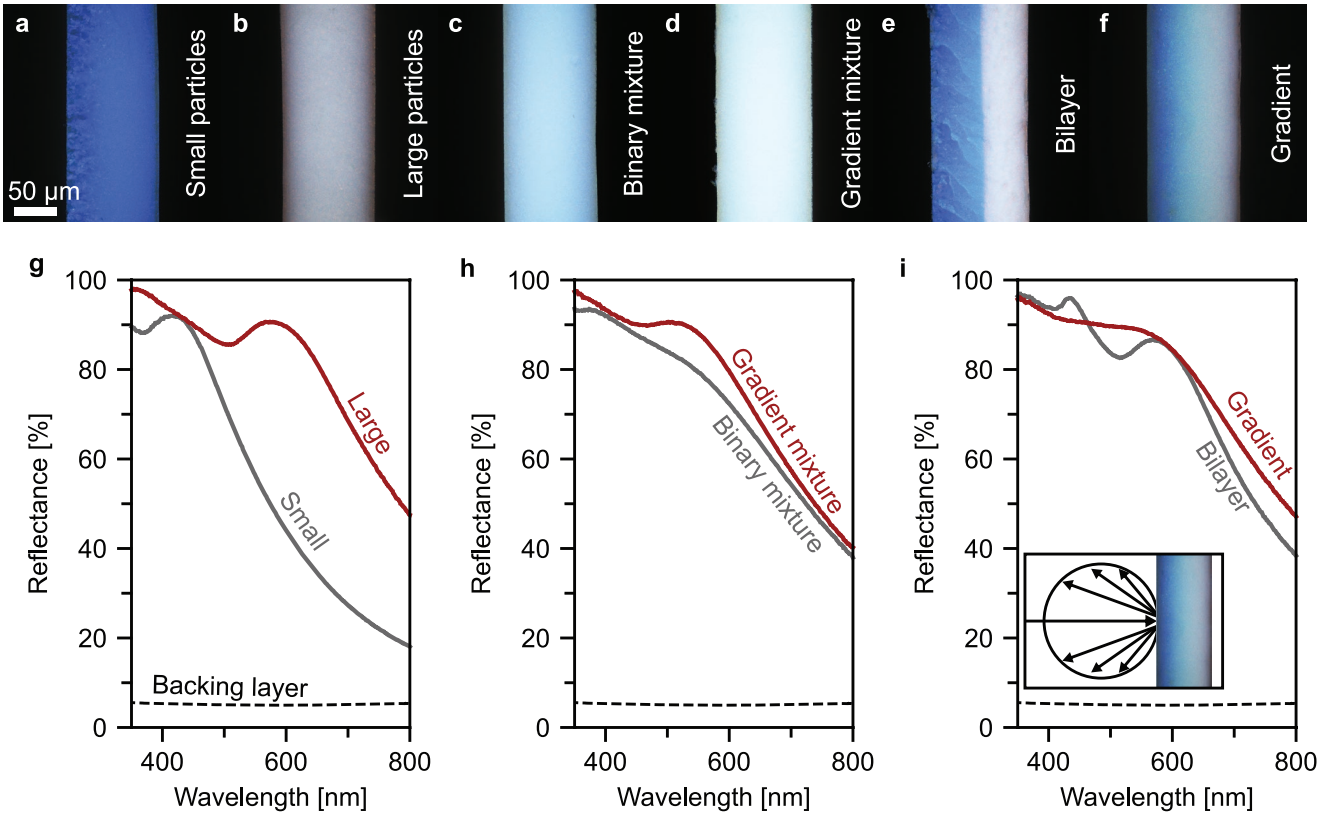

Figure 4. Diffuse reflectance UV–vis spectroscopy of colloidal assemblies prepared via filtration. a,b) Cross section light microscopy images of samples consisting of monodisperse particles. c) Disordered, binary mixture of these reference particles. d) Sample prepared by mixing all fractions obtained from the semibatch emulsion polymerization prior to filtration. e) Bilayer of small and large particles. f) Gradient sample prepared via the presented semicontinuous filtration approach after semibatch emulsion polymerization. g–i) UV–vis diffuse reflectance spectra of all samples measured with an integrating sphere. The inset in (i) elucidates the measurement geometry.

two pure SEM measurements show a statistical mixture of all particle sizes and no segregation (Figure S17, Supporting Information), corroborating that this coloration must be attributed to coherent scattering of the isotropic assembly. We rationalize the difference via the degree of disorder, elucidated by the pair distribution function, g(r) of the two types of colloidal glasses. Simple 2D simulations (Figure S18, Supporting Information) of both cases and subsequent g(r) evaluation[43] show that the binary mixture shows a pair correlation function limited to a set of distinct pairs: small–small, small–large, and large–large. No additional peaks can be observed in subsequent coordination spheres. In the gradient mixture, peaks in the g(r) can be observed up to the 5th coordination sphere. Since phase correlation and constructive interference of scattered waves depend on the short-range order[8] this results in a more pronounced peak in the reflectance spectrum.

Lastly, we compare the bilayer and the gradient sample (Figure 4i). The former represents the most extreme case of a stepwise gradient, while the latter is the fully continuous counterpart. In both cases, the sample is oriented, so that the smallest particles are on top. The reasoning behind this is that waves of shorter wavelengths (blue light) are affected more by diffuse scattering of the large particles. Small particles that show Mie resonance at these frequencies should, therefore, interact with the light first.[26] The spectrum of the bilayer shows two discrete peaks at the same wavelengths as the single-component reference samples. This proves that the diffuse reflectance measurements are sensitive to photons coherently scattered in lower regions of the sample. This is possible due to an increased ratio of single- and multiple scattering events caused by the short-range order and near-field effects.[13] These observations also hold for the interpretation of the optical properties of the gradient photonic glass. Here, we see a plateau over the full region between the two peaks of the bilayer. Unlike in the bilayer, no local minima and maxima are observed. Instead, a uniform reflectance results over the visible range. We attribute this unique property to the gradual mesoscale structure of this material. In comparison, step-gradient samples prepared via deposition of discrete layers always show distinct peaks (Figure S19, Supporting Information). The gradient spectrum is in accordance with the local optical characterization, as the plateau of the diffuse reflectance spans the same wavelength range as the maxima of peaks measured along the cross section in Figure 3b. Additionally, the plateau and general shape closely resemble the reflectance spectrum obtained from a non carbon-coated cross section measured with a large spot size (Figure S13c, Supporting Information). This implies the applicability of such a gradient material as a broadband reflector in a wavelength range of choice. We confirmed this possibility by a separate CrEEP synthesis with an

extended size range from 220 nm up to 450 nm (Figure S20, Supporting Information). The gradient colloidal glass, consequently, covers a much broader spectral range compared to the system outlined here (Figure S21, Supporting Information). The critical role of the mesoscopic structure becomes apparent when directly comparing the gradient superstructure to the gradient mixture (Figure S22, Supporting Information). Self-assembly of a gradient particle dispersion mixture without an additional mesoscopic gradient does not show a plateau in the visible range. Furthermore, the diffuse reflectance of the gradient photonic glass is superior to the disordered case across the entire spectral range.

Enhanced scattering of visible light is of great importance in fields such as thin reflective coatings and passive cooling applications.[44,45] Beside the use of high-n materials such as titania, recent studies have examined alternative approaches such as the variation of the particle morphology of low-n materials to improve the scattering performance.[21,46] An alternative/complementary approach is our optimized mesostructure. The gradient colloidal glass provides a tuneable approach to enhanced broadband reflectance, opening an alternative approach to create the whitest white. The fabrication proceeds without any stacking faults or cracks that can arise during the much more complicated fabrication of multilayer inverse opals or (2+1) photonic crystals.[15,25] Recent theoretical work has examined the passive cooling properties of gradient particulate assemblies.[33] These simulations are corroborated by our observation that the gradient colloidal glass shows superior diffuse reflectance compared to the mixed case. Overall, gradient mesostructures are a highly attractive materials class from which novel applications in the field of wave–matter interaction, granular mechanics, and filtration can be expected. This interest will be further expedited by the fact that this type of gradient can conceivably be assembled using any type of particle that can be fabricated via seeded growth.

3. Conclusion

We have introduced a general method that makes use of a previously untapped feature of colloid synthesis. The time-dependent growth of colloidal particles is stored in a thin extraction tube prior to self-assembly. The self-assembly process retains the gradual dispersion composition and provides access to fully continuous mesoscopic gradients. Local optical and structural characterization corroborated the gradient mesostructure, and diffuse reflectance measurements showcased the unique broadband reflectivity. Our method will be of immediate relevance for a broad interdisciplinary community investigating and optimizing photonic glasses toward highly efficient scattering systems[44,46] with potential applications in areas such as passive cooling.[45,47] Considering the generality of our synthetic approach, we expect that a wide range of novel, functional materials with a gradient composition will become available that reach far beyond model polymeric particles. Perfecting the self-assembly process may lead to elusive chirped colloidal crystals,[32,48] while infiltration can provide further insight as to the superior mechanical properties of composite and porous graded materials.[49,50]

4. Experimental Section

Materials: Water used in this work was of Millipore quality. Methyl methacrylate (MMA 99%), sodium styrene sulfonate (NaSS, 99.99%) and potassium persulfate (KPS, 99.99%) were obtained from Sigma Aldrich.

Seed Particle Synthesis: A 100 mL three-necked flask equipped with a reflux condenser and septa was loaded with 48 mL water and degassed for 75 min under a constant nitrogen stream at 80 °C and 650 rpm stirring speed. With 5 min of equilibration time between each addition, the following reactants are added: 1) 2 mg NaSS in 1 mL water, 2) 1.7 mL MMA, 3) 40 mg KPS in 1 mL water. The reaction was then allowed to proceed for 30 min before the semibatch process was initiated.

Semibatch Growth and Extraction: The setup preparation proceeds before the seed synthesis is started, so no oxygen enters the system between seed synthesis and gradual growth. Silicone tube (2 m) with an inner diameter of 2 mm was attached to a syringe, and both were filled with water. The free end of the tube was inserted through a septum and dipped into the reaction mixture. The cannula used for the injection of air was bent and inserted into this end of the tube. Two processes were started simultaneously after the 30 min of seed synthesis: 1) Monomer feed was initiated, and 3.0 mL MMA was added at 3.0 mL h^{-1}. 2) Extraction was initiated, and 5.0 mL were drawn into the tube at 5.0 mL h^{-1}. Air fractions of 16 µL were pumped into the tube end every 30 s. This resulted in 5–6 drops of monomer being added during the time it took to extract one fraction. After 60 min, 110 fractions were stored in the tube with a gradually increasing size of polymer latex particles. For the extended size range, the reaction proceeds analogously while adding 6.0 mL MMA at 6.0 mL h^{-1}. The introduction of air-bubbles to fractionate the extracted particle dispersion improved the particle size monodispersity during the filtration process (compare Figure S4, Supporting Information). It eliminated a boundary layer at the tube solid–liquid interface with zero flow velocity and quenches the polymerization. In combination with the laminar flow inside the tube any turbulent mixing was effectively suppressed by this technique and the extracted size distribution was retained.

Semicontinuous Filtration Assembly: The setup used for the filtration mediated self-assembly can schematically be seen in Figure S6 (Supporting information). The tube, filled with all fractions and still connected to the syringe, was used directly after the synthesis. Dispersion droplets were slowly pumped into an intermediate vessel at 0.4 mL h^{-1}. Water was simultaneously added dropwise at 60 mL h^{-1}. During dilution, the dispersion was mixed, and upon reaching a total volume of 5 mL, the vessel was periodically emptied via a Pythagorean cup mechanism. The diluted dispersion was thereby transferred into a vacuum filtration setup, and particles were deposited on a hydrophilized poly(tetrafluoroethylene) (PTFE) filter (Omnipore) with a pore size of 200 nm. The timing was adjusted, so that the filter process was completed before the next emptying of the intermediate vessel. During this time, the assembly did not dry but remained an aqueous paste. After completion, the swollen particle film was transferred from the filter via pressing and adhesion to a poly(dimethylsiloxane) (PDMS) substrate from which it could be removed after drying.

Reference samples were prepared via filtration of diluted dispersions of the seed particles and/or the particle dispersion remaining in the reaction vessel after the termination of the semibatch process.

Drop-Casting: Rapid self-assembly of every 10th fraction was done by direct drop-casting of 2 µL dispersion onto a clean glass substrate preheated to 80 °C.

Dynamic Light Scattering: Diluted dispersions were measured with a Zetasizer (Malvern) with 175° backscattering geometry to obtain the hydrodynamic diameter and the size distribution of the latex particles.

Viscosimetry: The relative viscosity of two dispersions with small (224 nm) and large (304 nm) particles in water was determined with an Ubbelohde viscosimeter at 30 °C. An Ubbelohde capillary type 0c in combination with a visco-clock was used to determine the flow times, respectively. The relative viscosity of the dispersion was calculated by $\eta_{\mathrm{Disp.}} = t(\eta_{\mathrm{H_2O}}/t_{\mathrm{H_2O}})$.

Carbon-Coating: A Leica EM ACE 600 coater with planetary stage and quartz crystal thickness measurement was used to deposit carbon nanolayers on the cross sections of samples with a sub-nanometer thickness accuracy.

Laser Scanning Confocal Microscopy: Both 2D color images, as well as 3D-reconstructed images, were obtained using a laser scanning confocal microscope (Olympus, OLS5000) with a white light source as well as a 405 nm laser, respectively. Cross sections were examined using a 50× lens with N.A. 0.95, and for the reconstruction, a pitch size of 0.12 µm was applied.

Scanning Electron Microscopy: Images were obtained with a Zeiss Leo 1530 (Carl Zeiss AG, Germany) at operating voltages of 1–3 kV and both in-lens as well as secondary-electron detection after sputtering of 2 nm of platinum.

Micro UV–vis Spectroscopy: UV–vis spectra of drop-cast suspensions were measured on an Olympus IX71 inverted microscope with a 4× lens (numerical aperture (NA) 0.10) in reflection geometry with a halogen light source. An OceanOptics USB4000 spectrometer was coupled via fiber optics.

The local measurements of the gradient cross section were conducted using a Zeiss Axio Imager Z2 light microscope with either a 20× lens (NA 0.5, EC Epiplan-NEOLFLUAR, Zeiss) or a 50× lens (NA 0.55, LD EC Epiplan-NEOFLUAR, Zeiss). Spectra were measured using an MCS CCD UV-NIR Spectrometer (Zeiss, Germany) coupled to the light microscope. The spot size was further adjusted using mechanical apertures in the optical path toward the detector. A silver mirror was used as reference.

Diffuse Reflectance Spectroscopy: Diffuse reflectance spectra were collected with a Cary 5000 UV–vis spectrometer (Agilent Technologies) in combination with an integrating sphere accessory (Labspheres). The samples were mounted at the reflectance port of the sphere after adhesion to a glass substrate with carbon adhesive tape. As a reference, a Spectralon diffuse white standard (Labspheres) was used.

2D Simulation of Particle Assemblies: 2D-rigid body physics of circles with different diameters falling into a rectangular basin were simulated using the Pymunk library in Python 3. Circles were initiated as dynamic bodies one after the other at a random x-position at the top of the plane. They experienced only downward directed gravitational force as well as rigid body interactions with other circles as well as the walls and floor of the basin. A total number of 4000 particles were simulated in each case in a basin measuring 1500 × 1000 units. The diameters were set to one of two specific integers (8 and 12) with a probability of 50% each for the binary case (Figure S18a,b, Supporting Information) and to random floating-point numbers between 8 and 12 for the mixed gradient case (Figure S18c,d, Supporting Information). The crystalline assembly was simulated by letting circles with a diameter of exactly 10 fall into the basin (Figure S18e,f, Supporting Information).

Supporting Information

Supporting Information is available from the Wiley Online Library or from the author.

Acknowledgements

N.V. acknowledges funding by the Deutsche Forschungsgemeinschaft (DFG, German Research Foundation) – Project-ID 416229255 – SFB 1411. M.S. and T.L. thank the Elite Network of Bavaria (ENB). The help from the Keylab Electron Microscopy is appreciated. This project has received funding from the European Research Council (ERC) under the European Union's Horizon 2020 research and innovation program (grant agreement no. #714968).

Open access funding enabled and organized by Projekt DEAL.

Conflict of Interest

The authors declare no conflict of interest.

Data Availability Statement

The data that support the findings of this study are available from the corresponding author upon reasonable request.

Keywords

colloidal self-assembly, gradient size distribution, light scattering, mesoscale gradients

Received: September 22, 2022
Revised: November 7, 2022
Published online: December 28, 2022

[1] J. D. Joannopoulos, P. R. Villeneuve, S. Fan, *Nature* **1997**, *386*, 143.
[2] S. John, *Phys. Rev. Lett.* **1987**, *58*, 2486.
[3] E. Ducrot, M. He, G. R. Yi, D. J. Pine, *Nat. Mater.* **2017**, *16*, 652.
[4] J. H. Holtz, S. A. Asher, *Nature* **1997**, *389*, 829.
[5] L. Maiwald, T. Sommer, M. S. Sidorenko, R. R. Yafyasov, M. E. Mustafa, M. Schulz, M. V. Rybin, M. Eich, A. Y. Petrov, *Adv. Opt. Mater.* **2021**, *10*, 2100785.
[6] Z. Hayran, H. Kurt, K. Staliunas, *Sci. Rep.* **2017**, *7*, 3046.
[7] Y. Takeoka, S. Yoshioka, A. Takano, S. Arai, K. Nueangnoraj, H. Nishihara, M. Teshima, Y. Ohtsuka, T. Seki, *Angew. Chem., Int. Ed.* **2013**, *52*, 7261.
[8] E. S. A. Goerlitzer, R. N. Klupp Taylor, N. Vogel, *Adv. Mater.* **2018**, *30*, 1706654.
[9] P. D. Garcia, R. Sapienza, A. Blanco, C. Lopez, *Adv. Mater.* **2007**, *19*, 2597.
[10] P. D. Garcia, R. Sapienza, C. Lopez, *Adv. Mater.* **2010**, *22*, 12.
[11] K. Ueno, A. Inaba, Y. Sano, M. Kondoh, M. Watanabe, *Chem. Commun.* **2009**, *24*, 3603.
[12] J. F. Galisteo-Lopez, M. Ibisate, R. Sapienza, L. S. Froufe-Perez, A. Blanco, C. Lopez, *Adv. Mater.* **2011**, *23*, 30.
[13] S. F. Liew, J. Forster, H. Noh, C. F. Schreck, V. Saranathan, X. Lu, L. Yang, R. O. Prum, C. S. O'Hern, E. R. Dufresne, H. Cao, *Opt. Express* **2011**, *19*, 8208.
[14] M. Harun-Ur-Rashid, A. Bin Imran, T. Seki, M. Ishii, H. Nakamura, Y. Takeoka, *ChemPhysChem* **2010**, *11*, 579.
[15] P. N. Dyachenko, J. J. do Rosário, E. W. Leib, A. Y. Petrov, R. Kubrin, G. A. Schneider, H. Weller, T. Vossmeyer, M. Eich, *ACS Photonics* **2014**, *1*, 1127.
[16] G. Shang, Y. Häntsch, K. P. Furlan, R. Janßen, G. A. Schneider, A. Petrov, M. Eich, *APL Photonics* **2019**, *4*, 046101.
[17] M. Retsch, M. Schmelzeisen, H. J. Butt, E. L. Thomas, *Nano Lett.* **2011**, *11*, 1389.
[18] S. Yu, C.-W. Qiu, Y. Chong, S. Torquato, N. Park, *Nat. Rev. Mater.* **2020**, *6*, 226.
[19] V. Hwang, A. B. Stephenson, S. Barkley, S. Brandt, M. Xiao, J. Aizenberg, V. N. Manoharan, *Proc. Natl. Acad. Sci. USA* **2021**, *118*, 2015551118.
[20] H. Yang, G. Jacucci, L. Schertel, S. Vignolini, *ACS Nano* **2022**, *16*, 7373.
[21] G. Jacucci, B. W. Longbottom, C. C. Parkins, S. A. F. Bon, S. Vignolini, *J. Mater. Chem. C* **2021**, *9*, 2695.
[22] N. Vogel, M. Retsch, C.-A. Fustin, A. del Campo, U. Jonas, *Chem. Rev.* **2015**, *115*, 6265.
[23] L. Zhang, J. Wang, S. Tao, C. Geng, Q. Yan, *Adv. Opt. Mater.* **2018**, *6*, 1701344.
[24] Y. Shen, D. Ye, I. Celanovic, S. G. Johnson, J. D. Joannopoulos, M. Soljačić, *Science* **2014**, *343*, 1499.

[25] L. Zhang, Z. Xiong, L. Shan, L. Zheng, T. Wei, Q. Yan, *Small* **2015**, *11*, 4910.
[26] R. Kubrin, R. M. Pasquarelli, M. Waleczek, H. S. Lee, R. Zierold, J. J. do Rosario, P. N. Dyachenko, J. M. Montero Moreno, A. Y. Petrov, R. Janssen, M. Eich, K. Nielsch, G. A. Schneider, *ACS Appl. Mater. Interfaces* **2016**, *8*, 10466.
[27] M. Chen, H. Colfen, S. Polarz, *ACS Nano* **2015**, *9*, 6944.
[28] J. Bahner, N. Klinkenberg, M. Frisch, L. Brauchle, S. Polarz, *Adv. Funct. Mater.* **2019**, *29*, 44.
[29] H. Ding, C. Liu, B. Ye, F. Fu, H. Wang, Y. Zhao, Z. Gu, *ACS Appl. Mater. Interfaces* **2016**, *8*, 6796.
[30] S. H. Kim, W. C. Jeong, H. Hwang, S. M. Yang, *Angew. Chem., Int. Ed.* **2011**, *50*, 11649.
[31] M. Schöttle, T. Tran, T. Feller, M. Retsch, *Adv. Mater.* **2021**, *33*, 2101948.
[32] J. S. Skibina, R. Iliew, J. Bethge, M. Bock, D. Fischer, V. I. Beloglasov, R. Wedell, G. Steinmeyer, *Nat. Photonics* **2008**, *2*, 679.
[33] Y. Fu, Y. An, Y. Xu, J. Dai, D. Lei, *EcoMat* **2022**, *4*, e12169.
[34] N. Vaidya, O. Solgaard, *Microsyst. Nanoeng.* **2022**, *8*, 69.
[35] F. A. Nutz, M. Retsch, *Sci. Adv.* **2017**, *3*, eaao5238.
[36] J. W. Goodwin, J. Hearn, C. C. Ho, R. H. Ottewill, *Colloid Polym. Sci.* **1974**, *252*, 464.
[37] J. Q. Li, R. Salovey, *J. Polym. Sci., Part A: Polym. Chem.* **2000**, *38*, 3181.
[38] F. J. Schork, W. H. Ray, *J. Appl. Polym. Sci.* **1987**, *34*, 1259.
[39] L. R. P. Areias, I. Mariz, E. Macoas, J. P. S. Farinha, *ACS Nano* **2021**, *15*, 11779.
[40] Y. Takeoka, M. Iwata, T. Seki, K. Nueangnoraj, H. Nishihara, S. Yoshioka, *Langmuir* **2018**, *34*, 4282.
[41] J. G. Park, S. H. Kim, S. Magkiriadou, T. M. Choi, Y. S. Kim, V. N. Manoharan, *Angew. Chem., Int. Ed.* **2014**, *53*, 2899.
[42] C. F. Bohren, D. R. Huffman, *Absorption and Scattering of Light by Small Particles*, John Wiley & Sons, New York, USA **1998**.
[43] B. A. F. Kopera, M. Retsch, *Anal. Chem.* **2018**, *90*, 13909.
[44] B. D. Wilts, X. Sheng, M. Holler, A. Diaz, M. Guizar-Sicairos, J. Raabe, R. Hoppe, S. H. Liu, R. Langford, O. D. Onelli, D. Chen, S. Torquato, U. Steiner, C. G. Schroer, S. Vignolini, A. Sepe, *Adv. Mater.* **2018**, *30*, 1702057.
[45] Q. Zhang, S. Wang, X. Wang, Y. Jiang, J. Li, W. Xu, B. Zhu, J. Zhu, *Small Methods* **2022**, *6*, e2101379.
[46] M. S. Toivonen, O. D. Onelli, G. Jacucci, V. Lovikka, O. J. Rojas, O. Ikkala, S. Vignolini, *Adv. Mater.* **2018**, *30*, 1704050.
[47] T. Wang, Y. Wu, L. Shi, X. Hu, M. Chen, L. Wu, *Nat. Commun.* **2021**, *12*, 365.
[48] B. Gates, Y. Xia, *Adv. Mater.* **2000**, *12*, 1329.
[49] C. Zhu, J. Qiu, S. Pongkitwitoon, S. Thomopoulos, Y. Xia, *Adv. Mater.* **2018**, *30*, 1706706.
[50] U. G. Wegst, H. Bai, E. Saiz, A. P. Tomsia, R. O. Ritchie, *Nat. Mater.* **2015**, *14*, 23.